INTERNATIONAL JOURNAL OF
INFORMATION AND SYSTEMS SCIENCES
Volume 2, Number 4, Pages 532-556



# MULTILEVEL PRECONDITIONING FOR 3D LARGE-SCALE SOFT-FIELD MEDICAL APPLICATIONS MODELLING

LIOR HORESH, MARTIN SCHWEIGER, MATTHIAS BOLLHÖFER, ABDEL DOUIRI, DAVID S. HOLDER AND SIMON R. ARRIDGE

**Abstract** Soft-field imaging methods, such as Optical Tomography (OT) and Electrical Impedance Tomography (EIT) have significant potential for medical imaging as they are non-invasive, portable and inexpensive. Possible clinical applications include epilepsy monitoring, cerebral stroke differentiation and screening for breast cancer. Recent advances in data acquisition instrumentation and image reconstruction algorithms raise the requirement to handle multiple large datasets from detailed large-scale geometric descriptions of biological objects. Thus, a major bottleneck lies in processing a large number of linear equations that result from the Finite-Element formulation of soft-field problems. Common numerical tools are not suited for large-scale problems, therefore alternative approaches are required. We propose the facilitation of an innovative multi-level inverse-based incomplete LU preconditioning approach to improve computational efficiency in processing EIT and OT system matrices. This combines static reordering and scaling, controlled growth of the inverse of triangular factors, and approximation of the Schur-complement in a multi-level scheme. Comparison with conventional incomplete LU factorisation provided a speed improvement of up to 11 times in preconditioner setup time, and up to 12 times in solution runtime for large-scale models. In addition, a new approach of monopolar current sources is introduced. Current sources and sinks are represented by linear combinations of a compact monopolar sources basis. Only the corresponding monopolar solutions are processed. These solutions serve as a basis for construction of the entire excitation pattern. This approach exploits the information content given in the system in an optimal manner and therefore avoids redundant computation.

**Key Words,** complex-valued, large-scale problems, soft-field, multi-level preconditioner, Krylov-subspace, monopolar sources, modelling, EIT, DOT, high order radiation transfer equation, $P_N$ approximation

## 1. Introduction

In the past two decades, there have been major advances in neuroimaging, with the development of hard-field imaging methods, such as MRI, X-ray CT and PET. In spite of their immense benefits, these are all expensive, immobile and image either anatomy or slow metabolic changes over time. An alternative are soft-field imaging methods, which may offer the advantages of portability, affordability and safety over their established hard-field counterparts. Two such methods, which are discussed in this paper, are: Optical Tomography (OT), in which reconstructed tomographic images of the optical properties are produced with arrays of optodes [1], and Electrical Impedance Tomography (EIT), in which images of the internal impedance of a subject are produced with an array of ECG type electrodes [2]. These methods are non-invasive, portable, inexpensive, and provide high temporal resolution of the order of tens of milliseconds. They offer the potential to

Received by the editors April 14, 2006

image blood volume and metabolic activity in a manner similar to fMRI or PET, with applications in long-term bedside monitoring required for progressing stroke, neonatal hypoxic-ischaemic brain injury, detection of epileptic seizure foci, lung respiration, breast cancer screening and gastric emptying monitoring. Under appropriate conditions, they could also provide uniquely useful methods for static imaging of acute cerebral stroke and breast cancer, where their cost and portability would allow them to be used in emergency or community conditions where large image acquisition systems are not practical.

Unfortunately, the advantages of soft-field imaging methods are offset by their limited spatial resolution and variability in reconstructed images. This limitation is described mathematically by the severe ill-posedness of the reconstruction problem. Physically, this is caused by the diffusive nature of the propagation of the fields and the resulting loss of high frequency spatial information. In the presence of measurement noise, the solution for these problems can become unstable. The inverse problem is also frequently underdetermined.

This limitation may be lessened by the addition of independent information and the imposition of a-priori knowledge onto the image reconstruction process. Recent advances in data acquisition partially reduce the ill-posedness of the problem by harnessing spectral information into the reconstruction process [3-5]. However, this requires calculation of more models or, alternatively, larger problems. Whilst the former can be addressed relatively easily using distributed computing [6;7], the latter still poses a major difficulty. Recent advances in modelling include the facilitation of realistic MRI/CT-based volume meshes [8-10]. This minimises geometric errors, which until recently were among the cardinal error contributors. Nevertheless, reliable and precise geometric representation of physiological organs is limited by the computational complexity of large-scale modelling. Over the years several attempts have been made to meet this computational challenge by the scalable approach of Geometric Multi-Grid [11;12]. Such an approach requires the construction of hierarchical domain meshes of decreasing resolution. While this is achievable for simple geometries, the complexity of real-life physiological models makes this task complicated at best, if possible at all. Head shape models for instance, include very thin layers, such as the Cerebrospinal Fluid (CSF), which cannot be coarsened geometrically without introducing significant errors. Moreover, mesh generation is a time-consuming process which cannot be performed automatically, and requires the services of a specialist. Algebraic Multi-Grid (AMG) is an alternative approach with benefits that have been widely reported and which avoids these drawbacks. However it is strictly derived for real-valued problems, which limits its application to a specific range of problems [13].

Other improvements in modelling involve better approximation of the governing equations, such as the employment of the Radiative Transfer Equation (RTE) for light transport [14-17], or accounting for the complete Maxwell equations set [18]. More accurate models however often lead to an increased problem size. Lastly, recent advances in algorithms include the development of effective non-linear iterative inverse solvers [10;19-22] which compensate well for the non-linearity of these problems, but require repeated calculation of the forward model for each of the non-linear iteration steps. Within each step, numerous evaluations of the forward model are required for the globalisation procedure such as line-search or trust regions methods [23;24].

A general method for handling complex-valued problems of growing scale is therefore required. This study proposes the employment of state of the art inverse-based multi-level algebraic preconditioner to handle large-scale problems [25]. We demonstrate the benefits

of such an approach by comparing its performance with the conventional approach of incomplete LU preconditioning for problems of growing scale and growing model complexity. In addition, a monopolar sources transformation is proposed for lossless soft-field imaging techniques. This approach reduces substantially the computational cost for both modelling and reconstruction purposes.

The paper is organised as follows: In section 2, the Finite Element formulation of the EIT and OT problems and conventional methods for solving the linear systems derived from this formulation are presented. In section 3, an alternative adaptation of the classical Algebraic Multi Grid (AMG) preconditioner for complex valued problems and the innovative multi-level inverse-based incomplete LU preconditioning approach are introduced. In section 4, a novel monopolar sources formulation for the EIT problem is presented. This approach is intended to reduce the computational burden associated with dipolar/multi-polar sources techniques. In sections 5 and 6, a numerical study that compares the computational demands of the suggested approaches with that of the conventional methods is presented. Finally, in section 7, we give some conclusions and in appendix 8 we provide a glossary.

## 2. Modelling Background

### 2.1. The governing equations

#### 2.1.1. EIT forward problem

In Electrical Impedance Tomography, the forward problem is to model the electric potential distribution inside a medium, due to injection of current from the boundary. The governing equations are Maxwell's equations in the quasi-static approximation together with the Neumann to Dirichlet mapping. Under these conditions, the time-harmonic Maxwell's equations reduce to the generalised Laplace equation, which provides the following relation for the electric potential

$$\nabla \cdot \left( \gamma(\mathbf{r};\omega) \nabla \mathrm{U}(\mathbf{r};\omega) \right) = 0 \qquad \mathbf{r} \in \Omega \tag{1}$$

where $\mathrm{U}$ is the scalar electric potential, $\gamma(\mathbf{r};\omega) = \sigma(\mathbf{r};\omega) + i\omega\varepsilon(\mathbf{r};\omega)$ is the electric admittivity coefficient tensor and $\omega$ is the angular frequency of the applied current. The integral of the current density over each electrode is equal to the total current $I_l$ driven to that electrode

$$\int_{e_l} \gamma \frac{\partial \mathrm{U}}{\partial v} dS = I_l \qquad \text{on } \partial\Omega_l \qquad l = 1, 2, ..., L \tag{2}$$

where $v$ is normal to the boundary $\partial\Omega$ and $e_l$ is the surface area of the electrode $l$. The electrode contact impedance is modelled by a thin layer with effective impedance $z_l$, the measured potential over the boundary $V_l$ is given by

$$\mathrm{U} + z_l \gamma \frac{\partial \mathrm{U}}{\partial v} = V_l \qquad \text{on } e_l \qquad l = 1, 2, ..., L \tag{3}$$

These relations are constrained by the current conservation condition

$$\sum_{l=1}^{L} I_l = 0 \tag{4}$$

For the sake of uniqueness a reference condition over the potential is added by grounding the potentials as follows

$$\sum_{l=1}^{L} V_l = 0 . \tag{5}$$

This formulation, namely the Complete Electrode Model [26;27], is the most accurate forward EIT model to date, and accounts for the effect of the electrodes' contact impedance (as opposed to its predecessor the Gap-Shunt model).

### 2.1.2. Optical Tomography forward problem

The forward problem in optical tomography requires modelling of light propagation in scattering media. Commonly, the Radiative Transport Equation is used which in the frequency domain is given by

$$\left( \hat{\mathbf{s}} \cdot \nabla + \mu_{tr}(\mathbf{r}) + \frac{i\omega}{c} \right) \mathrm{U}(\mathbf{r}, \hat{\mathbf{s}}; \omega) = \mu_s \int_{S^2} \Theta(\hat{\mathbf{s}}, \hat{\mathbf{s}}') \, \mathrm{U}(\mathbf{r}, \hat{\mathbf{s}}; \omega) \, d\hat{\mathbf{s}}' + q(\mathbf{r}, \hat{\mathbf{s}}; \omega) \tag{6}$$

where $\mathrm{U}(\mathbf{r}, \hat{\mathbf{s}}; \omega)$ is the number of photons per unit volume with angular direction $\hat{\mathbf{s}}$ at position $\mathbf{r}$, $\mu_s$ and $\mu_a$ are the scattering and absorption coefficients respectively, and $\mu_{tr} = \mu_s + \mu_a$ is the total attenuation in the angular direction. The modulation frequency is represented by $\omega$, $c$ is the speed of light, $q(\mathbf{r}, \hat{\mathbf{s}}; \omega)$ is the number of source photons and $\Theta(\hat{\mathbf{s}}, \hat{\mathbf{s}}')$ is the scattering kernel. Many approaches have been developed over the years to obtain solutions for the Radiative Transport Equation [15;28-30]; here we discuss the so-called $P_N$ method [14]. This approach involves expansion of an angular variable in Spherical Harmonics [1], and an approximation is provided by truncation of the spherical harmonics expansion at order N. The RTE is used when low-scattering domains are present. In the high-scattering regime, the model can be simplified to the diffusion equation with Robin boundary conditions. This approach is known as Diffuse Optical Tomography (DOT). The governing equations in this case in the frequency domain are

$$\begin{aligned} \left( -\nabla \cdot \kappa(\mathbf{r}) \nabla + \mu_a(\mathbf{r}) + \frac{i\omega}{c} \right) \mathrm{U}(\mathbf{r}, \omega) &= q(\mathbf{r}; \omega) && \mathbf{r} \in \Omega \\ \mathrm{U}(\xi; \omega) + 2\kappa\zeta \frac{\partial \mathrm{U}(\xi; \omega)}{\partial \nu} &= 0 && \xi \in \partial\Omega \end{aligned} \tag{7}$$

where $\kappa$ and $\mu_a$ are the diffusion and absorption coefficients respectively, $\mathrm{U}$ is the photon density distribution, $q$ is an isotropic source distribution, $\zeta$ is a boundary term which incorporates the refractive index mismatch at the tissue-air boundary, and $\nu$ is the outward normal of the boundary $\partial\Omega$ at $\xi$. The diffusion coefficient is related to the scattering coefficient $\mu_s$ by the following relation

$$\kappa = \frac{c}{3\left(\mu_a + (1 - \bar{\Theta})\mu_s\right)} . \tag{8}$$

where $\Theta$ is the average cosine of the phase function.

### 2.2. Finite Element Method (FEM) discretisation and matrix structure

Finite Element discretisation of the EIT or OT problem results in a linear set of equations. These systems are sparse, symmetric, non-Hermitian and indefinite. The spatial discretisation and approximation of the electric potential or the photon density by piecewise polynomial interpolation functions provides

$$\mathrm{U}^h(\mathbf{r},\omega)=\sum_{i=1}^{n}\phi_i(\mathbf{r})u_i(\omega) \tag{9}$$

where $u_i$ stand for the discrete sample of U at the i$^{\text{th}}$ node, $\phi_i$ are the basis function and $h$ represents a mesh discretisation parameter so that $\mathrm{U}^h \to \mathrm{U}$ when $h \to 0$. For the RTE an additional directional term is required in the representation

$$\mathrm{U}^h(\mathbf{r},\hat{\mathbf{s}};\omega)=\sum_{j}^{m}\sum_{i=1}^{n}\tilde{\phi}_{ij}(\mathbf{r},\hat{\mathbf{s}})u_i(\omega). \tag{10}$$

Often it is assumed that the basis can be developed separately for the spatial and angular terms

$$\tilde{\phi}_{ij}(\mathbf{r},\hat{\mathbf{s}})=\phi_i(\mathbf{r})\theta_j(\hat{\mathbf{s}}). \tag{11}$$

The $\mathrm{P_N}$ method takes the angular basis to be the spherical harmonics.

#### 2.2.1. EIT systems

Application of the above discrete approximation provides an augmented system matrix structure

$$\begin{pmatrix} A_M + A_Z & A_V \\ A_V^T & A_D \end{pmatrix}\begin{pmatrix}\mathbf{u}\\ \mathbf{v}\end{pmatrix}=\begin{pmatrix}\mathbf{0}\\ \mathbf{I}\end{pmatrix} \tag{12}$$

where

$$\begin{aligned}
A_M(i,j)&=\int_\Omega \gamma\nabla\phi_i\cdot\nabla\phi_j d\mathbf{r} && i,j=1:n_V;\ A_M\in\mathbb{C}^{n_V\times n_V}\\
A_Z(i,j)&=\sum_{l=1}^{n_L}\int_{e_l}\frac{1}{z_l}\phi_i\phi_j dS && i,j=1:n_V;\ A_Z\in\mathbb{C}^{n_V\times n_V}\\
A_V(i,l)&=-\int_{e_l}\frac{1}{z_l}\phi_i dS && i=1:n_V, l=1:n_L;\ A_V\in\mathbb{C}^{n_V\times n_L}\\
A_D(s,l)&=\begin{cases}\dfrac{1}{z_l}|e_l| & s=l\\ 0 & s\neq l\end{cases} && s,l=1:n_L;\ A_D\in\mathbb{C}^{n_L\times n_L}
\end{aligned} \tag{13}$$

where $n_V$ is the number of vertices and $n_L$ stands for the number of electrodes. The inner part $A_M + A_Z$, which corresponds to the Gap-shunt model, maintains the standard elliptic PDE structure and features and therefore can be regarded as an M-Matrix. However, the augmented parts $A_V$, $A_V^T$ and $A_D$ violate the M-matrix structure of the system [13]. The

right hand side (RHS) in EIT is typically composed of zeros apart from pairs of positive entries and their negations, representing the source and sink electrodes. This is due to the fact that current is not able to enter or leave any other site over the scalp other than from the injecting and receiving electrodes.

### 2.2.2. DOT discretisized systems

In a similar manner the discrete representation of the diffusion $\kappa$ and absorption $\mu_a$ coefficients over (7) provides

$$\left(K(\kappa)+C(\mu_a)+A+i\omega B\right)\mathbf{u}(\omega)=\mathbf{q}(\omega) \tag{14}$$

where $\mathbf{u}(\omega),\mathbf{q}(\omega)\in\mathbb{R}^n$ and the system matrices $K,C,A,B\in\mathbb{R}^{n\times n}$ are given by

$$\begin{aligned} K_{ij} &= \int_{\Omega}\kappa(\mathbf{r})\nabla\phi_i(\mathbf{r})\cdot\nabla\phi_j(\mathbf{r})\,d\mathbf{r} \\ C_{ij} &= \int_{\Omega}\mu_a(\mathbf{r})\phi_i(\mathbf{r})\phi_j(\mathbf{r})\,d\mathbf{r} \\ A_{ij} &= \frac{1}{2\zeta}\int_{\partial\Omega}\phi_i(\mathbf{r})\phi_j(\mathbf{r})\,d\mathbf{S} \\ B_{ij} &= \frac{1}{c}\int_{\Omega}\phi_i(\mathbf{r})\phi_j(\mathbf{r})\,d\mathbf{r} \end{aligned} \tag{15}$$

Each of these matrices is symmetric, and therefore so is their weighted sum. Whenever the frequency $\omega>0$, the argument $i\omega B$ in (14) contributes imaginary entries to the system, which implies that the global coefficient system is complex valued and indefinite. For the specific case where $\omega=0$, the coefficient system is Symmetric Positive Definite (SPD) and satisfies the M-Matrix properties.

### 2.2.3. $P_N$ expansion for Optical Tomography discretisized systems

Since the global structure represents the spatial expansion, the global coefficient system $\mathbf{P}_N$ derived from the $P_N$ approximation has the same sparse and symmetric structure as the diffusion approximation. The separation of variables in the basis function expansion implies that only the inner structure is altered, consequently, each of the entries in the diffusion approximation system matrix is replaced by a block $P_N$ matrix, which represents the directional expansion in spherical harmonics up to the truncation order N

$$\mathbf{P}_N\mathbf{u}(\mathbf{r};\omega)=\mathbf{q}(\mathbf{r};\omega) \tag{16}$$

where

$$\mathbf{P}_N=\begin{pmatrix} D_0 & A_0 & 0 & 0 & \cdots \\ A_0^T & 3D_1 & 3A_1 & 0 & \cdots \\ 0 & 3A_1^T & 5D_2 & 5A_2 & \cdots \\ & & & & \cdots \\ \vdots & \vdots & \vdots & \vdots & \ddots \end{pmatrix} \tag{17}$$

Each block matrix $D_i \in \mathbb{C}^{(2i+1)\times(2i+1)}$ is diagonal for angularly independent scattering

$$D_1 = \left( \mu_a + (1-\Theta_l)\mu_s + \frac{i\omega}{c} \right) I_1 \tag{18}$$

and the i[th] block $A_i \in \mathbb{C}^{(2i+1)\times(2i+3)}$ is a sparse matrix representing a generalisation of the divergence operator [31]

$$A_1 = \begin{bmatrix} \alpha_{l,-l} D_\xi^+ & \beta_{l,-l} \dfrac{\partial}{\partial z} & \gamma_{l,-l} D_\xi^- & 0 & \cdots \\ 0 & \alpha_{l,1-l} D_\xi^+ & \beta_{l,1-l} \dfrac{\partial}{\partial z} & \gamma_{l,1-l} D_\xi^- & \cdots \\ \vdots & \vdots & \vdots & \vdots & \vdots \\ \cdots & 0 & \alpha_{l,l} D_\xi^+ & \beta_{l,l} \dfrac{\partial}{\partial z} & \gamma_{l,l} D_\xi^- \end{bmatrix} \tag{19}$$

where

$$\begin{aligned} \alpha_{l.m} &= \sqrt{(l-m+2)(l-m+1)} \Big/ (2l+1) \\ \beta_{l.m} &= \sqrt{(l-m+1)(l+m+1)} \Big/ (2l+1) \\ \gamma_{l.m} &= \sqrt{(l+m+1)(l+m+2)} \Big/ (2l+1) \\ D_\xi^{+(-)} &= \frac{-1}{2} \left( \frac{\partial}{\partial x} + (-) i \frac{\partial}{\partial y} \right) \end{aligned} .$$

Consequently, the dimensions of the coefficient matrix are proportional to $(N+1)^2/2$. Higher order models therefore lead to rapid growth in the system size, which introduces a major computational problem for large-scale models.

## 3. Preconditioning

### 3.1. Introduction

Systems derived from large-scale models are typically approached by Krylov-subspace iterative solvers, such as stabilised Bi-Conjugated Gradients (BiCGstab) [32] or Generalised Minimum Residual (GMRes) [33]. For the specific case of real valued systems, which represent the purely resistive case for EIT (ERT), or the DC case of OT, the coefficient system $A$ is Symmetric Positive Definite (SPD), which permits the usage of the Krylov-subspace Preconditioned Conjugated Gradients (PCG) solver [34].

Error convergence and stability of Krylov-subspace methods depends strongly on the spectrum of the system. The more clustered the eigenvalues of $A$, the more rapid and stable the convergence becomes. The complex geometry of realistic physiological models, and in particular head models, imposes strict constraints over the model discretisation regularity. Among the various mesh quality measures, variations in element volume and small angled elements impair the system conditioning. Furthermore, the heterogeneous nature of the physical parameters scatters the eigenvalues of the system even further [35]. These two aspects lead to the requirement for appropriate preconditioning.

Preconditioning is a process in which the linear system is transformed into an equivalent system (in the sense that it has the same solution), but that has more favourable spectral properties, i.e. its eigenvalues are better clustered. A preconditioner $M$ is a matrix that effect such transformation

$$M^{-1}Ax = M^{-1}b \,. \tag{20}$$

A good preconditioner possesses the following properties: for any vector $v$, $M^{-1}v$ can be obtained easily, and $M^{-1}A$ is close to an identity matrix. A conventional choice is to form the preconditioner by incomplete factorisation of the original system. The most common choice for preconditioning complex valued indefinite systems is by incomplete LU decomposition, in which the system matrix $A \in \mathbb{C}^{n\times n}$ is decomposed into a product of a lower triangular matrix $L$ and an upper triangular matrix $U$

$$A = LU + \mathcal{E} \tag{21}$$

where $\mathcal{E}$ is the error due to the factorisation incompleteness. The control over the completeness of these factors is done through selection of a drop tolerance parameter $\eta$. There is a trade-off between the computational effort required for factorisation and the effectiveness of the preconditioner, which is manifested by the solution runtime. This preconditioning approach is highly effective, yet, its computational demand grows rapidly with problem scale. This poses a limitation for its employment for realistic problems.

An alternative approach for solving linear systems is the Algebraic Multi-Grid method (AMG) [36]. The motivation is rooted in the limitation of stationary relaxation schemes (also known as smoothers), such as Jacobi or Gauss-Seidel, to reduce the low-frequency components of the error. These schemes effectively damp the high frequency components of the error, while leaving the low-frequencies almost unaffected. In order to address this difficulty, AMG suggests the construction of a hierarchy of system matrices, along with a set of prolongation and restriction operators which map between them. The algorithm works in a recursive manner, starting by applying relaxation over the system, followed by application of restriction over the residual error. The next step is a recursive call, where the restricted residuals serve as the right hand side for the restricted system. This procedure is followed down to the lowest (i.e. coarsest) level, where a correction for the error is solved directly. From then on, this correction is interpolated using the prolongation operators and added to the solution at each level, usually with the application of another post-relaxation stage.

While used as a solver over classical elliptic PDE problems with M-matrix structure, the computational demand is optimal, i.e. scales like $\mathcal{O}(n)$. However, it is most effective as a preconditioner for an iterative solver, rather than for providing a complete solution.

### 3.2. The classical AMG preconditioner

Soleimani et al [13] suggested the utilisation of commercial classical AMG [37] as a preconditioner for the ERT problem (real valued EIT). They postulated that the augmented section of the ERT system (13) invalidates only slightly the M-matrix definition, and therefore permits the use of a classical blackbox multi-grid preconditioner for the real valued problem. This approach indeed demonstrated a significant speedup in the forward solution stage. However, in cases where these conditions are not met, such as at low or high frequency where contact impedance values are extreme, in non-linear applications where the conductivity approaches zero while approaching the solution, or in the common

case for medical applications where permittivity cannot be ignored, more advanced techniques are required. Note that for real symmetric SPD problems such as resistive EIT or DC DOT, a symmetric smoother is required, which is not a property of classical smoothers in their standard form. For the complex valued case, an unsymmetrical technique is required which is discussed in the next section.

### 3.3. The modified unsymmetrical classical AMG preconditioner

An elegant way to provide a multi-level preconditioner using the classical AMG formulation for complex valued matrices is by a complex-to-real splitting and construction of an implicit AMG preconditioner. The first step is conversion of the symmetric complex matrix into real valued non-symmetric system

$$Ax = (C + iB)\,x = b \Rightarrow \begin{pmatrix} \mathrm{C} & B \\ -B & C \end{pmatrix} \begin{pmatrix} \mathrm{x}_{\Im \mathrm{m}} \\ \mathrm{x}_{\Re \mathrm{e}} \end{pmatrix} = \begin{pmatrix} \mathrm{b}_{\Im \mathrm{m}} \\ \mathrm{b}_{\Re \mathrm{e}} \end{pmatrix} \tag{22}$$

where $C, B \in \mathbb{R}^{n \times n}, b \in \mathbb{C}^{n \times 1}$ and $C$ is approximately an M-matrix. Such a system (like its complex equivalent) could be solved using Krylov-subspace solvers which are suitable for non-symmetric matrices, such as stabilised BiCGstab, GMRES or QMR. Let us consider first the following preconditioner

$$M = \begin{pmatrix} C & B \\ 0 & C \end{pmatrix} \tag{23}$$

At each nonsymmetric solver's iteration the system $My = z$ is needed to be solved. This can be done by rewriting the system as

$$\begin{pmatrix} C & B \\ 0 & C \end{pmatrix} \begin{pmatrix} y_{\Im \mathrm{m}} \\ y_{\Re \mathrm{e}} \end{pmatrix} = \begin{pmatrix} z_{\Im \mathrm{m}} \\ z_{\Re \mathrm{e}} \end{pmatrix} \tag{24}$$

At this stage, the following procedures could be performed in order to solve the system

$$\text{solve } Cy_{\Re \mathrm{e}} = z_{\Re \mathrm{e}} \tag{25}$$

$$\text{solve } Cy_{\Im \mathrm{m}} = z_{\Im \mathrm{m}} - By_{\Re \mathrm{e}} \tag{26}$$

These internal solution procedures can be performed by any method, such as CG. However, unlike $C + iB$, $C$ is approximately an M-matrix, therefore, classical AMG can be employed here. While using an iterative method in (25) and (26), the required accuracy tolerance question needs to be addressed. Classical multi-grid is a stationary method; therefore, application of a single AMG V-cycle rather than an accurate solution suffices [38]. In this case, the preconditioner becomes

$$\hat{M} = \begin{pmatrix} \hat{C} & B \\ 0 & \hat{C} \end{pmatrix} \tag{27}$$

where $\hat{C}$ is defined by the V-cycle, and therefore not formed explicitly. Nevertheless, although this approach can be used for wider range of applications, it is still prone to solution convergence breakdown, whenever the approximation of the system matrix to an

M-matrix is violated. In addition, the complex-to-real-split process doubles the storage requirements of the system matrix, which for large-scale systems can be limiting.

### 3.4. Inverse-based multi-level ILU preconditioning

Bollhöfer and Saad [25] recently introduced the innovative approach of inverse-based multi-level preconditioning. Unlike other multi-level preconditioning approaches, this approach is capable of handling complex valued sparse matrices of general structure, as well as efficiently handling Hermitian and symmetric structures. The algorithm comprises three core stages. At the first stage rescaling and static partial reordering is applied to define a well-suited leading block $B$. Then the coefficient system entries are being permuted to reduce the level of fill-in in the factorisation

$$A \to P^T AQ = \begin{pmatrix} B & F \\ E & C \end{pmatrix} \tag{28}$$

where $P$ and $Q$ are permutation matrices, $B$ is the leading matrix block and $C$, $E$ and $F$ are the remaining block matrices. The next stage is a partial incomplete LU factorisation with diagonal pivoting. At this stage $P^T AQ$ is factored so that the growth of its inverse triangular factors is bounded by $\left\| \mathcal{L}^{-1} \right\|, \left\| \mathcal{U}^{-1} \right\| \le \tau$, using a factor and skip strategy (Figure 1)

$$P^T AQ \to \hat{P}^T A\hat{Q} = \begin{pmatrix} \hat{B} & \hat{F} \\ \hat{E} & \hat{C} \end{pmatrix} = \underbrace{\begin{pmatrix} L_B & 0 \\ L_E & I \end{pmatrix}}_{\mathcal{L}} \underbrace{\begin{pmatrix} D_B & 0 \\ 0 & S_C \end{pmatrix}}_{\mathcal{D}} \underbrace{\begin{pmatrix} U_B & U_F \\ 0 & I \end{pmatrix}}_{\mathcal{U}}. \tag{29}$$

The norms of these factors are related to the factorisation error term. Analysis shows that the incomplete LU factorisation resulting from dropping small entries in Gaussian elimination produces a good preconditioner when the inverses of these factors have norms that are not too large [39]. Therefore, at each step, rows or columns that exceed a prescribed bound are pushed to the end, as illustrated in Figure 1.

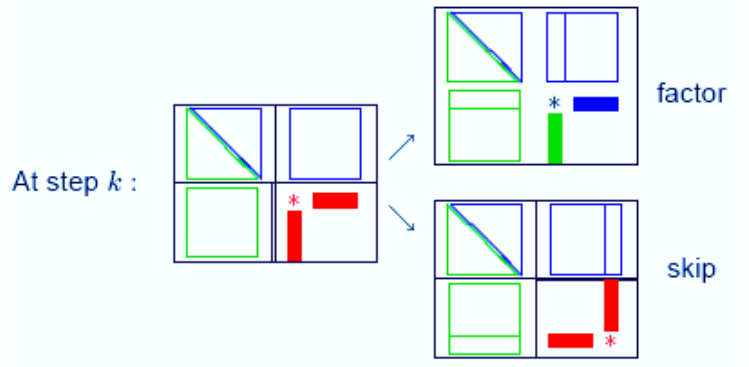


**Figure 1. An illustration of the factor and skip strategy at level k, rows or columns which exceed the prescribed bounds are omitted from the incomplete factorisation and moved towards the lower right part of the system matrix [40]**

The last step is incorporation of the scheme above in a multilevel manner, so that the

sub-matrix which was skipped from the factorisation will be treated on the next level (Figure 2). Thus, a multi-level strategy is applied recursively to the approximate Schur complement $S_c$ of the system at each level

$$A \xrightarrow{1} P^T A Q \xrightarrow{2} \hat{P}^T A \hat{Q} \xrightarrow{3} \begin{pmatrix} LDU & F \\ E & S \end{pmatrix}$$
$$S \xrightarrow{1} P_S^T S Q_S \xrightarrow{2} \hat{P}_S^T A \hat{Q}_S \xrightarrow{3} \begin{pmatrix} L_S D_S U_S & F_S \\ E_S & T \end{pmatrix} \qquad (30)$$
$$\vdots$$

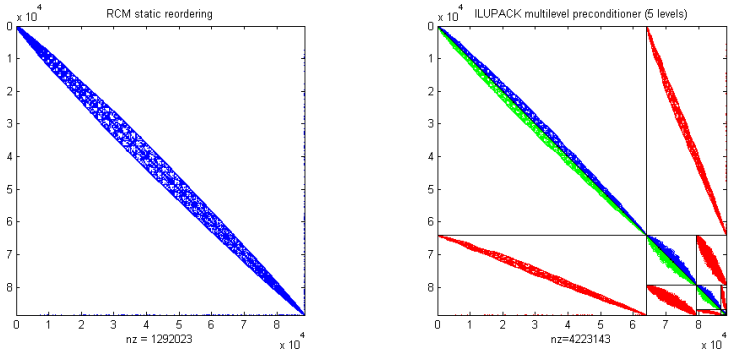


**Figure 2. Large-scale EIT system matrix of 90k × 90k entries. Left: single level Reverse Cuthill McKee (RCM) ordering; Right: the same matrix after inverse-based multi-level partitioning**

An implementation of this framework is available in the ILUPACK [40] package. Expanded functionality, and in particular a broader variety of reordering schemes can be obtained by linking this package with the parallel sparse direct linear solver Pardiso [41-43]. The package also includes a selection of Krylov solvers, including the recent Flexible Generalised Residual (FGMRes) algorithm [44] and facilitates the use of the more robust Symmetric (Simplified) Quasi Minimum Residual (SQMR) [45], rather than the conventional stabilised Bi-CG for symmetric indefinite systems [46].

## 4. Monopolar current excitation

The right-hand sides of DOT systems include the distribution of the sources only, with no sinks. However, EIT was so far modelled by a composition of sources and sinks, as derived from the stringent current conservation physical limitation. Nevertheless, mathematically, this limitation is not compulsory. Let $A \in \mathbb{C}^{n \times n}$ be the system matrix and $X = \{x^1, ..., x^v\} \in \mathbb{C}^{n \times v}$ a set of solutions corresponding to the set of lossless soft-field RHS column vectors $B = \{b^1, ..., b^v\} \in \mathbb{R}^{n \times v}$, which together forms the following set of linear systems

$$AX = B \qquad (31)$$

where a typical RHS term satisfies

$$\begin{aligned} \sum_i b_i^j &= 0 \qquad 1 \le i \le n \\ \sum_i \left| b_i^j \right| &\neq 0 \quad 1 \le j \le \nu \end{aligned} . \tag{32}$$

In the most general case, each column vector $b^j$ will include a composition of a few positive entries and their negations. Modern acquisition systems would allow multiple excitation patterns, involving the usage of each source numerous times with different sinks. For such cases, the number of unique excitation patterns exceeds the number of unique sources and sinks. Let us denote by $Q = \left\{ q^1, ..., q^s \right\} \in \mathbb{R}^{n \times s}, s \le \nu$ the subset of unit basis vectors that spans the column space of $B$, and by $P = \left\{ \alpha_1, ..., \alpha_\nu \right\} \in \mathbb{R}^{s \times \nu}$ the corresponding coordinate matrix transformation

$$b^j = \sum_{i \le s} \alpha_i^j q^i \tag{33}$$

or in matrix notation

$$B = QP . \tag{34}$$

Thus, the linear system can now be rewritten as

$$AX = QP . \tag{35}$$

Assuming $A$ is invertible, and since matrix multiplication is associative, one has

$$X = A^{-1}\left(QP\right) = \underbrace{\left(A^{-1}Q\right)}_{\tilde{Q}} P \tag{36}$$

where $\tilde{Q}$ are the solutions for the monopolar sources given by

$$\tilde{q}^i \equiv A^{-1} q^i . \tag{37}$$

Then one finally obtains

$$x^j = \sum_{i \le s} \alpha_i^j \tilde{q}^i \tag{38}$$

$$X = \left(X^T\right)^T = \left(P^T \left(A^{-1}Q\right)^T\right)^T . \tag{39}$$

Since $A$ is a linear operator, each solution vector $x^j$, which corresponds to a RHS $b^j$ term, can be also decomposed into $s$ linear combinations $\tilde{q}^i$, each of which is the solution for a monopolar source $q^i$. Hence, only a solution of the system for each of the RHS elementary basis vectors $q^i$ is required in order to construct any solution as a simple linear combination.

With the growing cost of computation for each solution $x^j$, and the relatively low computational cost of vector summation whenever $s < \nu$ there will be a clear benefit of almost a factor of $\nu / s$ in speedup by employing this approach. This approach bounds the number of forward solutions for a given coefficient system to be the number of unique independent sources (for EIT this would be the number of electrodes). If we consider simulation studies, where a complete dipolar excitation pattern is employed, this approach will reduce the computational cost from $n_L\left(n_L - 1\right)/2$ to $n_L$, i.e. it requires about twice of the square root of the original number of systems to be solved. In some respects, this

approach provides the most compact form of representing the total amount of independent information which resides in the system.

## 5. Numerical testing

Assessment and quantification of the benefits of employing the inverse-based multi-level ILU preconditioning scheme were performed over three types of complex valued matrices: EIT, DOT and $P_N$ systems. After test matrices were generated, a comparison with a conventional preconditioner based on incomplete LU factorisation and conventional solvers (stabilised Bi-CG and GMRes) was performed.

### 5.1. Generation of EIT test system matrices

Six realistic MRI-based adult head shape volume meshes of four layers each (scalp, skull, cerebrospinal fluid (CSF) and brain) were generated [8]. (Figure 3, left). The models consisted of logarithmically growing number of elements with 12k, 31k, 53k, 136k, 262k and 503k elements, and with 3k, 6k, 10k, 25k, 48k and 90k vertices respectively. The coarsest and finest meshes are shown in Figure 3 middle and right.

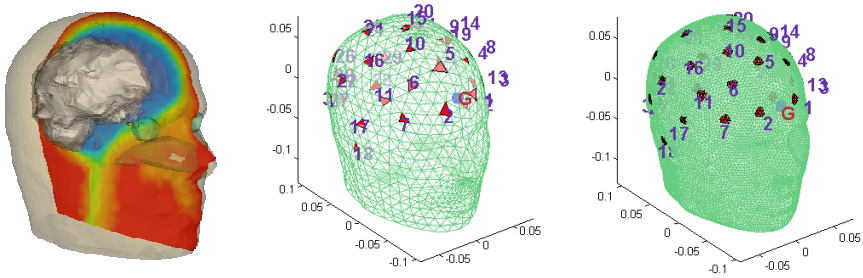

**Figure 3. Left: Multi - shell Finite Elements head model; Middle: coarsest model 12k elements, 3k nodes. Right: finest model 503k elements, 90k nodes. Red markings represent the electrode injection sites, and the G marks represent the grounding electrode**

Admittivity values of normal human head tissues at the frequency of 75Hz were assigned to the model [47]. 31 electrodes were positioned over the scalp according to the extended EEG 10-20 positioning, and a complete non-reciprocal dipolar current injection protocol with current level of 100μA was used. Contact impedance of 1kΩ was set for all electrodes. These parameters were passed into the UCL EIT group SuperSolver [48] to generate complex valued symmetric system matrices and their corresponding RHS. The SuperSolver employs a modified version of EIDORS 3D [49] for generating the coefficients matrix. Reverse Cuthill McKee (RCM) nodal reordering was applied to all systems.

### 5.2. Generation of DOT test system matrices

In a similar manner, three MRI-based neonate head shape meshes containing four layers were generated (Figure 4). Models were of 14k, 100k, and 760k elements, and 3k, 19k and 140k vertices respectively. 21 optodes were equally distributed over the neonate models' scalps. Absorption and scattering coefficients for normal neonate head tissues were assigned at each node [10]. The public domain package TOAST [50] was used to obtain complex valued Finite Element coefficient matrices from linear basis functions. The same

reordering scheme as in section 5.1 was applied.

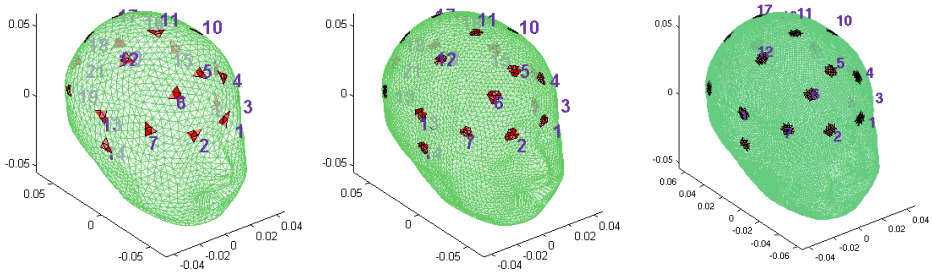

**Figure 4. Finite Element neonate head meshes. The models consisted 14k, 100k and 740k elements, and 3k, 19k and 140k vertices respectively. Red marks represent optodes locations**

### 5.3. Generation of $P_N$ test system matrices

$P_N$ systems matrices were generated using the smallest mesh discretisation for $P_1$, $P_3$, $P_5$ and $P_7$ approximations, resulting in system matrices of dimensions 4k, 16k, 40k and 75k. Similarly for the denser mesh $P_1$ and $P_3$ matrices were generated, with corresponding system matrices of size 19k and 112k. Lastly a $P_1$ system matrix of the densest mesh model was generated (140k).

### 5.4. Preconditioners and solvers evaluation

The derived complex valued systems were preconditioned with the following methods: a) Matlab's incomplete LU factorisation [51]. b) Complex-to-real splitting with implicit classical AMG preconditioning. c) ILUPACK inverse-based multi-level incomplete LU preconditioning with Maximum Weight Matching (MWM) rescaling and RCM reordering [42;52].

The solution procedure was performed in the following manners: a) stabilised BiCG (Matlab) preconditioned by standard incomplete LU based preconditioner. b) GMRes (Matlab) preconditioned by standard incomplete LU based preconditioner. c) stabilised BiCG (Matlab) preconditioned by complex-to-real splitting with implicit classical AMG preconditioner. d) SQMR (ILUPack) with multi-level inverse-based preconditioner. The latter was compared with an in-house Matlab implementation of the SQMR solver to eliminate platform and code architecture efficiency dependence.

For all solvers, the maximum number of iterations was set to 500, and desired relative residual error $\|Ax_k - b\|_2 / \|b\|_2 \le \varepsilon$ levels of $10^{-6}$, $10^{-9}$, and $10^{-12}$ were attempted. These choices for relative residual errors were derived from the expected acquisition noise levels and the wide dynamic range of the data [1;53]. ILUPack solvers employ the backward error criterion $\|Ax_k - b\| < \varepsilon\left(\|A\|\|x_k\| + \|b\|\right)$, and therefore were adjusted to comply with Matlab's relative residual error criterion mentioned above to allow fair comparison. The actual relative residual error obtained from each solution procedure, along with the runtime and total number of iteration was monitored. Bounds for the inverse triangular factors from the incomplete LU decomposition were set by the 'condest' parameter to 10 for the EIT and DOT approximations, and to 20 for the $P_N$ problems.

All incomplete factorisation based preconditioners were formed with drop tolerances $\eta$ of $10^{-2}$ and $10^{-3}$. This choice was taken after initial experimentation in order to provide minimal complete runtime for a coefficient matrix with about 20-30 RHS commonly used

for the type of imaging problems here considered. Storage requirement was recorded by the relative non-zeros (nnz) population in the preconditioner versus the original matrix, i.e. $nnz(preconditioner)/nnz(A)$. The comparison was performed with a dual Xeon 2.8 GHz, 2GB RAM workstation on a single processor mode with Debian Linux and Matlab 7.1 [53].

## 6. Numerical results and Discussion

In this section we study some aspects of the performance of different methods for the three kinds of large-scale modelling problems presented in section 5. We look in particular at the growth in time and space complexity of the preconditioners and the solvers.

Only the results for relative residual tolerance $10^{-12}$ are presented. The runtime results for the higher relative residual error of $10^{-6}$ and $10^{-9}$ were qualitatively similar to these, and therefore are not presented.

### 6.1. EIT systems

**Factorisation**

The construction of the multi-level inverse-based preconditioner was faster than the conventional incomplete LU factorisation, in particular for larger model sizes. It provided speedup factors of up to 3.4 and 6 for the higher and lower drop tolerances respectively (Figure 5). This behaviour is expected, due to the overhead required for construction of a multi-level hierarchy which, for smaller models, negates its benefit. Even so, the incresing speedup factor with the problem scale indicates the superiority of the multi-level approach in runtime complexity.

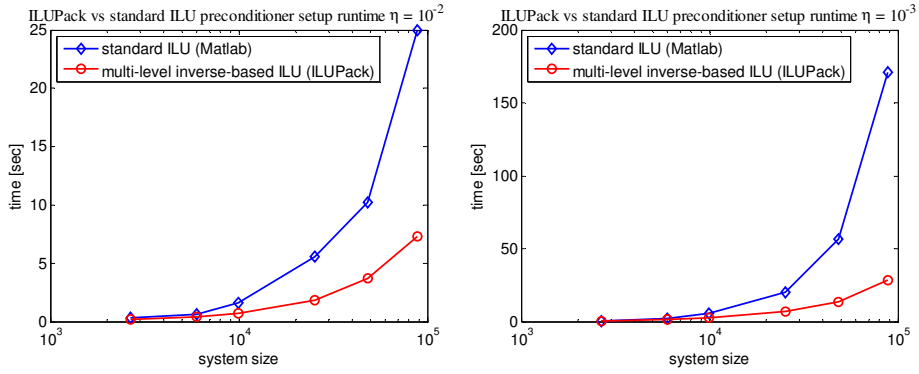


**Figure 5. Complex valued EIT systems factorisation runtime. Left: drop tolerance of $10^{-2}$; Right: drop tolerance of $10^{-3}$**

**Solution runtime**

The fastest convergence was obtained with the SQMR solver with multi-level inverse-based preconditioning and Maximum Weight Matching. Its speed advantage over the stabilised BiCG with conventional incomplete LU based preconditioning increased with problem size. It provided a convergence runtime speedup of up to 12 and 7.6 for the higher and lower drop tolerance accordingly (Figure 6). GMRes preconditioned with incomplete LU failed to converge for the 2nd, 5th and 6th larger systems. Stabilised BiCG with complex-to-real splitting with implicit classical AMG preconditioner failed to converge for the 4th and 6th systems. A possible cause is the violation of the M-matrix

structure in the Complete Electrode Model. This claim is further strengthened by the fact that this approach worked successfully for the complex-valued DOT systems which comply with the M-matrix definition requirements. A direct runtime comparison with results obtained using the splitting transformation (3.3) of the classical AMG is difficult. At first glance, the runtime seems excessively larger than that obtained using the conventional or inverse-based alternatives. However, this approach requires only multi-level SPD system setup, which for these systems is up to 2 and 9 times faster than complex-valued multi-level preconditioning and incomplete LU factorisation respectively. Whenever this approach indeed converged, its overall runtime for a single RHS is still better than that of the conventional use of incomplete LU preconditioning. However, for multiple RHS, which is the common practice for most imaging problems, there will be a crossing point where the use of a conventional incomplete LU preconditioner will be more efficient.

An interesting point is the smoother convergence runtime with respect to the problem scale, offered by the inverse-based factorisation. This property can be attributed to the strict control over the factor growth with respect to the inverse error.

A runtime comparison between GMRes and SQMR solvers with Matlab implementation versus ILUPack implementation showed that the latter was faster by a factor of up to 1.5. This step was performed to quantify the effect of implementation and software architecture over runtime, and therefore, assesses that the effective speedup owed to inverse-based preconditioning in neutral conditions is about 8 and 5 for the higher and lower drop tolerance respectively.

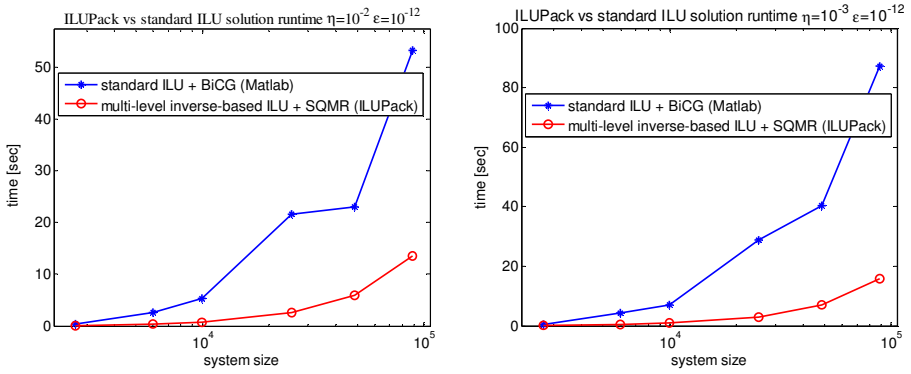


**Figure 6. Complex valued EIT systems solution runtime. Left: drop tolerance of $10^{-2}$; Right: drop tolerance of $10^{-3}$**

## Memory requirement

For the higher drop tolerance, the inverse-based preconditioner memory requirement was lower than for incomplete LU preconditioner for all problems scales by up to 12%. However, for the lower drop tolerance, the former required more storage by up to 30% (Table 1). These results are somewhat surprising, as, typically, the memory requirements of multi-level techniques are expected to be consistently greater than those of a single level. Nevertheless, these results show that it is possible to construct a multi-level preconditioner which is less populated than a single level one, as long as the entries which are affecting the inverse error are bounded properly.

## 6.2. DOT systems

### Factorisation

Construction of the multi-level inverse-based preconditioner was increasingly faster than performing incomplete LU factorisation by a speedup factor of up to 5.4 for both drop tolerances (Figure 7).

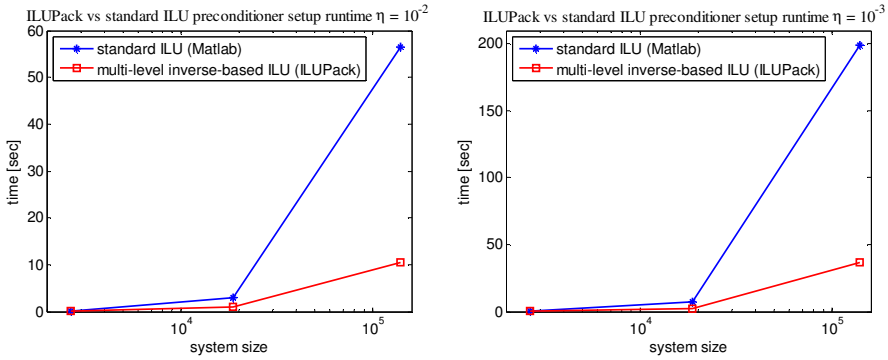


**Figure 7. Complex valued DOT systems factorisation runtime. Left: drop tolerance of $10^{-2}$; Right: drop tolerance of $10^{-3}$**

### Solution runtime

SQMR with the multi-level inverse-based preconditioner provided the fastest convergence runtime, with speedup factor of up to 3.8 and 2.8 with respect to the stabilised BiCG algorithm using a conventional preconditioner based on the incomplete LU factorisation (Figure 8). Unlike in the EIT case, this time both GMRes and the complex-to-real splitting transformation with the implicit classical AMG preconditioner converged properly. Yet, their runtime scaled worse with the problem size. As the modified AMG preconditioning scheme requires only a multi-level real valued preconditioner, its complete runtime for a single RHS is still substantially better than that of the conventional use of incomplete LU preconditioner. Similarly, as in the EIT case, this advantage holds as long as the number of RHS is small.

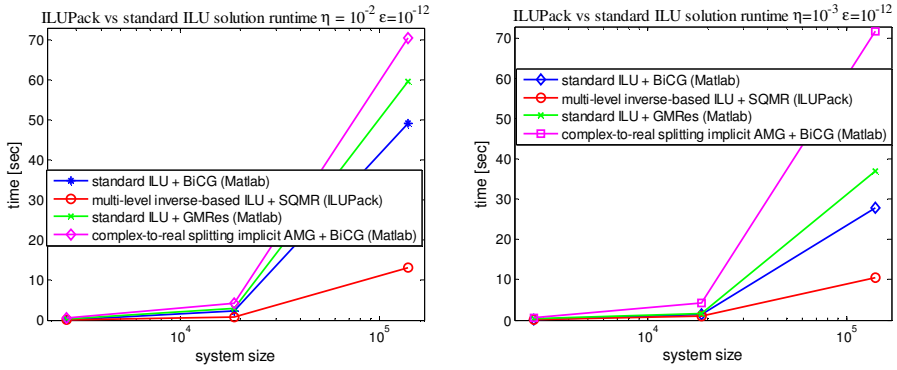


**Figure 8. Complex valued DOT systems solution runtime. Left: drop tolerance of $10^{-2}$; Right: drop tolerance of $10^{-3}$**

**Memory requirement**

Storage requirements for the multi-level inverse-based preconditioner grew consistently larger over the problem scale with respect to the conventional incomplete LU factorisation. While for the smallest model the storage requirement of the former was about half of the latter, for the largest model it became larger by a factor of 1.8 and 1.2 for the higher and lower drop tolerances respectively (Table 1).

## 6.3. $P_N$ matrices

**Factorisation**

Inverse-based preconditioner construction was faster than standard incomplete LU factorisation by an increasing speedup factor from 1.8 to 9 and 2.6 to 11.1 with the approximation order N (for the smaller model $P_1$ to $P_7$ approximations) for the higher and lower drop tolerance respectively. A similar trend can be seen for the convergence speedup of the medium size model ($P_1$ and $P_3$ systems), which was increasing from 3 to 6.3 and from 3.4 to 7.1 for the lower and higher drop tolerances respectively (Figure 9). Whilst the setup runtime of the former was about linear with the matrix dimension and super-linear with the approximation order, for the latter it grew at a quadratic rate. These results are of special significance, as the intensive computational demands related to preconditioning of realistic size $P_N$ systems set a major limitation for the radiation and optics communities.

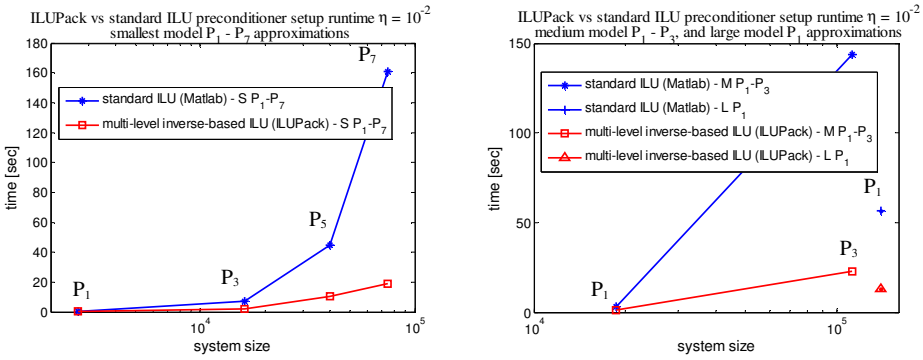


**Figure 9. Complex valued $P_N$ systems factorisation runtime with drop tolerance of $10^{-2}$. Left: smallest model $P_1$ - $P_7$; Right: medium $P_1$ - $P_3$ and largest $P_1$ models**

**Solution runtime**

SQMR with inverse-based multi-level factorisation was up to 4.7 and 3.9 times faster than BiCGstab or GMRes with standard incomplete LU preconditioner for growing $P_N$ order, for the higher and lower drop tolerances respectively. Memory limitations, did not allow assessing this assertion for the larger models up to the same approximation order. Yet, the runtime speedup growth between the $P_1$ and $P_3$ approximations for the medium size model grew from 1.4 to 2.1 and from 9.2 to 9.4 for the higher and lower drop tolerances respectively. The largest model was attempted only for the lowest approximation order, which provided speedup factors of 3.2 and 4.3 (Figure 10). These results indicate that the inverse-based preconditioning scheme can precondition this special structured matrices better than the conventional approaches in use.

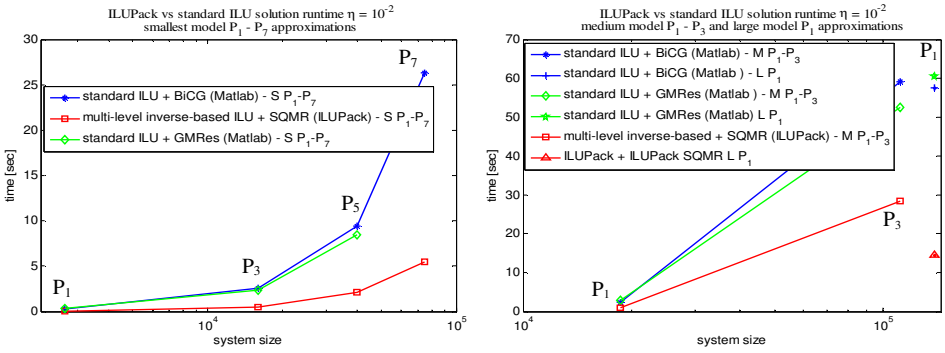


**Figure 10. Complex valued $P_N$ systems solution runtime with drop tolerance of $10^{-2}$. Left: smallest model (S) $P_1$ - $P_7$. GMRes with conventional incomplete LU preconditioner failed to converge for the $P_7$ system, and therefore was omitted from the graph; Right: medium (M) $P_1$ - $P_3$ and largest (L) $P_1$ models**

## Memory requirement

Preconditioner relative size grew larger with the model size, in a similar manner as in the EIT and DOT cases. Conversely, for increasing approximation order, the relative preconditioner storage requirements grew significantly smaller. This trend is common for both preconditioners with both drop tolerances. A comparison of the preconditioners relative population, with respect to the increasing approximation order N, showed that the inverse based preconditioner consumed a decreasingly smaller portion of memory over its conventional counterpart. The former was 1.9 to 4.7 and 1.6 to 2.1 times smaller than the latter for the smaller model $P_1$ to $P_7$ for the higher and lower drop tolerances respectively. Similar trends were observed for the larger models as well. These results indicate that there is a trade-off between the faster growth in memory requirement due to the increase in model dimensions and the decrease in the relative population due to the increasing order of approximation (Table 1).

The application of Maximum Weight Matching yielded marginal differences in iteration count and in runtime. The system matrices presented in this study have diagonally dominant structure, and therefore cannot be improved substantially by this scheme. Nevertheless, $P_N$ systems are governed by block structures, which distribute the dominance of the near diagonal region, therefore, a custom-made matching scheme that can exploit the block structure of these matrices, may provide better results.

**Table 1. Memory requirement summary for each of the preconditioning approaches**

| | *Size* $[n]$ | *Average row sparsity* $\left\lfloor \frac{nnz(A)}{n} \right\rfloor$ | *Sparsity* $\left\lfloor \frac{nnz(A)}{n^2} \right\rfloor$ | *Incomplete LU* $\left\lfloor \frac{nnz(L)+nnz(U)-nnz(D)}{nnz(A)} \right\rfloor$ | | *Inverse-based multi-level ILU* $\left\lfloor \frac{\sum_l nnz(L_l)+nnz(U_l)-nnz(D_l)}{nnz(A)} \right\rfloor$ | |
|---|---|---|---|---|---|---|---|
| | | | | $\eta=10^{-2}$ | $\eta=10^{-3}$ | $\eta=10^{-2}$ | $\eta=10^{-3}$ |
| EIT | 2668 | 13.07 | 0.0049 | 1.51 | 4.49 | 1.7 | 4.03 |
| | 5970 | 13.73 | 0.0023 | 1.34 | 3.80 | 1.69 | 3.69 |
| | 9955 | 13.94 | 0.0014 | 1.35 | 3.81 | 1.75 | 3.77 |
| | 25200 | 15.12 | 0.0006 | 1.58 | 4.37 | 1.73 | 3.84 |
| | 48425 | 14.53 | 0.0003 | 1.4 | 4.05 | 1.74 | 3.92 |
| | 88523 | 17.7 | 0.0002 | 1.42 | 4.26 | 1.85 | 4.26 |
| DOT | 2668 | 13.07 | 0.0049 | 1.18 | 2.30 | 0.62 | 1.33 |
| | 18653 | 13.06 | 0.0007 | 1.44 | 3.38 | 1.56 | 3.72 |
| | 139397 | 13.94 | 0.0001 | 1.63 | 4.21 | 1.92 | 7.44 |
| $P_1$ | 2668 | 13.07 | 0.0049 | 1.18 | 2.3 | 0.62 | 1.44 |
| $P_3$ | 15996 | 75.18 | 0.0047 | 0.46 | 1.46 | 0.23 | 0.84 |
| $P_5$ | 39990 | 159.96 | 0.004 | 0.21 | 1.02 | 0.1 | 0.58 |
| $P_7$ | 74648 | 246.34 | 0.0033 | 0.14 | 0.76 | 0.03 | 0.36 |
| $P_1$ | 18653 | 13.06 | 0.0007 | 1.44 | 3.38 | 1.48 | 3.57 |
| $P_3$ | 111918 | 78.34 | 0.0007 | 0.61 | 1.93 | 0.53 | 1.61 |
| $P_1$ | 139397 | 13.94 | 0.0001 | 1.63 | 4.2 | 2.24 | 5.8 |

## 7. Conclusions

In this paper we presented two approaches for reducing the computational demand of large-scale soft-field forward problems: the use of virtual monopolar sources, which bounds the number of required solutions of lossless soft-field techniques by the number of sources, and the facilitation of the novel inverse-based multi-level ILU preconditioning approach. This approach was compared with several conventional strategies for preconditioning large-scale sparse system matrices which arise from soft field forward modelling of medical applications.

For the complex symmetric systems that were tested in this study, the symmetric variant of the Maximum Weight Matching (MWM) reordering scheme was marginally better in iteration count and runtime. Our prior knowledge regarding the block structure of the $P_N$ systems can be further exploited in order to provide better preconditioning schemes.

Regarding the solvers compared in this study, the SQMR solver provided smoother, faster and more stable convergence than the conventional stabilised BiCG or GMRes.

Of the preconditioners studied, the inverse-based multi-level ILU preconditioner provided superior runtime both in terms of construction and solution convergence. Two

factors affect this behaviour: the degree of ill-conditioning of the problem and the problem scale. The control over the prescribed bound for the norm of the inverse triangular factors can be derived from an estimate for the ill-conditioning of the system. Whenever the system is more ill-conditioned, this scheme provides greater speedup. Whilst for small-scale problems the benefits of this approach are not significant, at large-scales this preconditioning framework requires substantially lower runtimes than the leading conventional approaches.

We have found inverse-based preconditioning effective for the EIT and OT problems discussed in this paper. A future topic of study could be their application to other soft field methods, such as Magnetic Induction Tomography (MIT). Finally, another important subject for future work would be evaluation of the performance of inverse-based multi-level preconditioner in parallel architecture mode.

## 8. Appendix: Definitions of terms

### 8.1.1. Positive definiteness

A matrix $A \in \mathbb{C}^{n\times n}$ is called positive definite if for any non-zero complex valued vector $x \in \mathbb{C}^n$ if the following holds

$$\mathrm{Re}\left(x^* Ax\right) > 0 \tag{40}$$

where $x^*$ stands for the conjugate transpose of $x$.

### 8.1.2. M-matrix

A matrix $A \in \mathbb{R}^{n\times n}$ is defined as M-matrix if

$$\begin{aligned} A_{ii} &> 0 \qquad i = 1:n \\ A_{ij} &\le 0 \qquad i, j = 1:n \quad i \ne j \end{aligned} \tag{41}$$

and for some positive diagonal matrix $D$, $AD$ is strictly diagonally dominant

$$\left|(AD)_{ii}\right| \ge \sum_{j=1, j\ne i}^{n} \left|(AD)_{ii}\right| \tag{42}$$

### 8.1.3. Schur complement

For matrices $B^{p\times p}, F^{p\times q}, C^{q\times p}$ and $D^{q\times q}$ that compose the system

$$A = \begin{pmatrix} B & F \\ C & D \end{pmatrix} \tag{43}$$

the Schur complement of the block $D$ of a matrix is defined as

$$S_c \equiv B - FD^{-1}C \tag{44}$$

### 8.1.4. Ill-conditioning

Matrix is said to be ill-conditioned if its eigenvalues are widely scattered. Conversely, matrix with clustered eigenvalues is well-conditioned.

## 9. Acknowledgements

The authors wish to thank Prof. E. Haber from Emory University for his guidance and assistance in developing the modified unsymmetrical multi-level preconditioning method for complex valued systems, A. Tizzard from Middlesex University and R. Schindmes from University College London for producing MRI-based Finite-Element meshes, D. Poccecai from University College London for his support in computational resourcing, and special thanks for UCL Graduate School, Universities UK and EPSRC grant GR/R86201/01 for funding.

## 10. References

[1] S. R. Arridge, "Optical tomography in medical imaging," *Inverse problems*, Vol.15, no. 2, p. R41-R93, 1999.

[2] D. S. Holder, Electrical Impedance Tomography: Methods, history and applications. University College London, UK: IoP, 2005.

[3] A. McEwan, A. Romsauerova, R. J. Yerworth, L. Horesh, R. H. Bayford, and D. S. Holder, "Design and calibration of a compact multi-frequency EIT system for acute stroke imaging," *Physiol. Meas*, Vol.27, no. 5, p. S199-S210, 2006.

[4] M. Mayer, P. Brunner, R. Merwa, F. M. Smolle-Jüttner, A. Maier, and H. Scharfetter, "Direct reconstruction of tissue parameters from differential multifrequency EIT in vivo," *Physiol. Meas*, Vol.27, no. 5, p. S93-S101, 2006.

[5] A. Corlu, T. Durduran, R. Choe, M. Schweiger, E. M. Hillman, S. R. Arridge, and A. G. Yodh, "Uniqueness and wavelength optimization in continuous-wave multispectral diffuse optical tomography," *Opt. Lett*., Vol.28, no. 23, pp.2339-2341, 2003.

[6] J. Fritschy, L. Horesh, D. S. Holder, and R. H. Bayford, "Using the GRID to improve the computation speed of electrical impedance tomography (EIT) reconstruction algorithms," *Physiol. Meas*., Vol.26, no. 2, p. S209-S215, 2005.

[7] J. Fritschy, L. Horesh, D. S. Holder, and R. H. Bayford, "Applications of GRID in clinical neurophysiology and Electrical Impedance Tomography of brain function," *Stud. Health Technol. Inform*., Vol.112, pp.138-145, 2005.

[8] A. Tizzard, L. Horesh, R. J. Yerworth, D. S. Holder, and R. H. Bayford, "Generating accurate finite element meshes for the forward model of the human head in EIT," *Physiol. Meas*., Vol.26, no. 2, p. S251-S261, 2005.

[9] C. R. Johnson and D. M. Weinstein, "Biomedical computing and visualization,", 48 ed. V. Estivill-Castro and G. Dobbie, Eds. Twenty-Ninth Australasian Computer Science Conference (ACSC2006), Hobart, Australia. Conferences in Research and Practice in Information Technology (CRPIT): 2006, pp.3-10.

[10] A. H. Barnett, A. G. Culver, A. Soresend, A. Dale, and D. A. Boas, "Robust Inference of Baseline Optical Properties of the Human Head with 3D Segmentation from Magnetic Resonance Imaging," *Appl. Optics*, Vol.42, pp.3095-3108, 2003.

[11] Y. Yao, Y. Wang, Y. Pei, W. Zhu, J. Hu, and R. L. Barbour, "Frequency domain optical tomography in human tissue,", 2570 ed. R. Barbour, M. Carvlin, and M. Fiddy, Eds. Experimental and Numerical Methods for Solving Ill-Posed Inverse Problems: Medical and Nonmedical Applications: 1995, pp.254-266.

[12] L. Borcea, "A nonlinear multigrid for imaging electrical conductivity and permittivity at low frequency," *Inverse problems*, Vol.17, no. 2, pp.329-359, 2001.

[13] M. Soleimani, C. E. Powell, and N. Polydorides, "Improving the forward solver for the complete electrode model in EIT using algebraic multigrid," *IEEE Trans. Med. Imaging*, Vol.24, no. 5, pp.577-583, 2005.
[14] E. D. Aydin, C. R. de Oliveira, and A. J. Goddard, "A comparison between transport and diffusion calculations using a finite element-spherical harmonics radiation transport method," *Med. Phys.*, Vol.29, no. 9, pp.2013-2023, 2002.
[15] A. D. Klose, U. Netz, J. Beuthan, and A. H. Hielscher, "Optical tomography using the time-independent equation of radiative transfer - Part 1: Forward model," *J. Quantitative Spectroscopy and Radiative Transfer*, Vol.72, pp.691-713, 2002.
[16] S. Wright, M. Schweiger, and S. R. Arridge, "Optical tomographic reconstruction using the Pn radiative transfer equations,", 3 ed 5th international conference on inverse problems in engineering: 2005, p. w04.
[17] M. Schweiger and S. R. Arridge, "Solutions to the transport equations using variable order angular basis," *International society for optical engineering (SPIE)*, Vol.5859, no. Photon Migration and Diffuse-Light Imaging II, pp.160-167, 2005.
[18] N. K. Soni, K. D. Paulsen, H. Dehghani, and A. Hartov, "Image reconstruction in Electrical Impedance Tomography using the full set of Maxwell's equations," VI International Conference on Biomedical Applications of Electrical Impedance Tomography, London, UK, 2005.
[19] L. Horesh, M. Schweiger, S. R. Arridge, and D. S. Holder, "Large Scale Non-Linear 3D Reconstruction Algorithms for Electrical Impedance Tomography of the Human Brain," Applied Inverse Problems Conference, Royal Agricultural College, Conference Centre, UK: 2005.
[20] V. Kolehmainen, M. Vauhkonen, P. A. Karjalainen, and J. P. Kaipio, "Assessment of errors in static electrical impedance tomography with adjacent and trigonometric current patterns," *Physiol. Meas.*, Vol.18, no. 4, pp.289-303, 1997.
[21] M. Molinari, S. J. Cox, BH Blott, and GJ Daniell, "Efficient non-linear 3D Electrical Tomography reconstruction 2," in ISBN 0 85316 2247, 2nd World Congress on Industrial Process Tomography ed Hannover, Germany: 2001.
[22] M. Molinari, H. Fangohr, J. Generowicz, and S. J. Cox, "Efficient non-linear 3D Electrical Tomography reconstruction 1," in ISBN 0 85316 2247, 2nd World Congress on Industrial Process Tomography ed Hannover,Germany: 2001.
[23] C. R. Vogel, Computational Methods for Inverse Problems SIAM, Philadelphia, 2002.
[24] W. H. Press, S. A. Teukolsky, W. T. Vetterling, and B. P. Flannery, Numerical recipes in C - The art of scientific computing, Second Edition ed. Cambridge New York Port Chester Melbourne Sydney: Press Syndicate of the University of Cambridge, 2002.
[25] M. Bollhöfer and Y. Saad, "Multilevel preconditioners constructed from inverse-based ILUs," *SIAM J. Sci. Comput.*, Vol.27, no. 5, pp.1627-1650, 2006.
[26] P. J. Vauhkonen, M. Vauhkonen, T. SaVolainen, and J. P. Kaipio, "Three-dimensional electrical impedance tomography based on the complete electrode model," *IEEE Trans. Biomed. Eng*, Vol.46, no. 9, pp.1150-1160,1999.
[27] E. Somersalo, M. D. Cheney, and D. Isaacson, "Existence and uniqueness for electrode models for electric-current Computed-Tomography," *SIAM J. Appl. Math*, Vol.52, no. 4, pp.1023-1040, Aug.1992.
[28] G. Bal and Y. Maday, "Coupling of transport and diffusion models in linear transport theory," *ESAIM: Mathematical Modelling and Numerical Analysis*, Vol.36, no. 1, pp.69-86, 2001.
[29] T. Tarvainen, M. Vauhkonen, V. Kolehmainen, S. R. Arridge, and J. P. Kaipio, "Coupled radiative transfer equation and diffusion approximation model for photon migration in turbid medium with low-scattering and non-scattering regions," *Phys. Med. Biol.*, Vol.50, no. 20, pp.4913-4930, 2005.
[30] T. Tarvainen, M. Vauhkonen, V. Kolehmainen, and J. P. Kaipio, "Hybrid radiative-transfer-diffusion model for optical tomography," *Appl. Optics*, Vol.44, no. 6, pp.876-886, 2005.

[31] S. Wright, S. R. Arridge, and M. Schweiger, "A Finite Element Method for the even-parity Radiative Transfer Equation using the PN approximation," "Numerical methods for multidimensional radiative transfer problems". Kanschat G., Meinköhn E., Rannacher R., and Wehrse R., Eds. Berlin: Springer, 2006.

[32] H. Van der Vorst, "Bi-CGSTAB: A Fast and Smoothly Converging Variant of Bi-CG for the Solution of Nonsymmetric Linear Systems," *SIAM J. Sci. Statist. Comput.*, Vol.13, pp.631-644, 1992.

[33] Y. Saad and M. H. Schultz, "GMRes: A generalized minimal residual algorithm for solving nonsymmetric linear systems," *SIAM J. Sci. Statist. Comput.*, Vol.7, pp.856-869, 1986.

[34] R. Barrett, M. Berry, T. F. Chan, J. Demmek, J. M. Donato, J. Dongarra, V. Eijkhout, P. Roldan, C. Rommie, and H. Van der Vorst, Templates for the Solution of Linear Systems: Building Blocks for Iterative Methods SIAM, 1994.

[35] J. R. Shewchuk, "What is a good linear element? Interpolation, conditioning, and quality measures,", 11th international Meshing Roundtable ed Sandia National Laboratories: Ithaca, New York, 2002, pp.115-126.

[36] A. Brandt, S. McCormick, and J. W. Ruge, "Algebraic multigrid (AMG) for automatic multigrid solution with application to geodetic computations,"POB - 1852, 1982.

[37] J. W. Ruge and K. Stuben, "Algebraic Multigrid," *SIAM Multigrid Methods*., Vol.4, no. Frontiers in Appl. Math, pp.73-131, 1987.

[38] W. L. Briggs, V. E. Henson, and S. F. McCormick, A Multigrid tutorial, 2nd ed SIAM, 2002.

[39] M. Bollhöfer and Saad.Y., "On the relations between ILU s and factored approximate inverses," *SIAM J. Matrix Anal. Appl*., Vol.24, no. 1, pp.219-237, 2002.

[40] M. Bollhöfer, Y. Saad, and O. Schenk, "ILUPACK - preconditioning software package,", Available online at http://www.math.tu-berlin.de/ilupack/, Release V2.1, January ed 2006.

[41] O. Schenk, K. Gärtner, and W. Fichtner, "Efficient sparse LU factorization with left-right looking strategy on shared memory multiprocessors," *BIT*, Vol.40, no. 1, pp.158-176, 2000.

[42] O. Schenk and K. Gärtner, "Solving unsymmetric sparse systems of linear equations with PARDISO," *Journal of Future Generation Computer Systems*, Vol.20(3), no. 475, p. 487, 2004.

[43] O. Schenk and K. Gärtner, "On fast factorization pivoting methods for sparse symmetric indefinite systems," Department of Computer Science, University of Basel,CS-2004-004, 2004.

[44] Y. Saad, "A flexible inner-outer preconditioned GMRes algorithm," *SIAM J. Sci. Stat. Comput.*, Vol.14, pp.461-469, 1993.

[45] R. W. Freund and N. M. Nachtigal, "A new Krylov-subspace method for symmetric indefinite linear systems,", 94-07 ed 1994.

[46] R. W. Freund and N. M. Nachtigal, "QMR Quasi Minimal Residual method for non-Hermitian linear systems," *Numer. Math*, Vol.60, pp.315-339, 1991.

[47] L. Horesh, A. Romsauerova, O. Gilad, A. McEwan, S. R. Arridge, and D. S. Holder, "Review of the dielectric properties of the human head for Multi-Frequency Electrical Impedance Tomography (MFEIT)," (In press) 2006.

[48] L. Horesh, O. Gilad, A. Romsauerova, A. McEwan, S. R. Arridge, and D. S. Holder, "Stroke type differentiation by Multi-Frequency Electrical Impedance Tomography (MFEIT) - A feasibility study,", 11 ed 3rd European Medical and Biological Engineering Conference, Prague, Czech Republic, 2005:

[49] N. Polydorides and W. R. Lionheart, "A Matlab toolkit for three-dimensional electrical impedance tomography: a contribution to the Electrical Impedance and Diffuse Optical Reconstruction Software project," *Meas. Sci. Technol.*, Vol.13, no. 12, pp.1871-83, 2002.

[50] M. Schweiger and S. R. Arridge, "TOAST - Time-resolved Optical Absorption and Scattering Tomography,", Available online at http://www.medphys.ucl.ac.uk/~martins/toast/index.html ed 2006.

[51] Y. Saad, "Iterative methods for sparse linear systems - Preconditioning techniques,", 2nd ed SIAM, 2003.

[52] S. Röllin and O. Schenck, "Maximum-weighted matching strategies and the application to symmetric indefinite systems,", Lecture Notes in Computer Science LNCS 3732 ed 2005, pp.808-817.

[53] Mathworks LTD, "Matlab the language of numerical computing," Mathworks, 2006.

Lior Horesh, UCL/Medical Physics, Neurophysiology, London, UK
Email: l.horesh@ucl.ac.uk

Martin Schweiger, UCL/Computer Science, CMIC, London, UK

M. Bollhöfer, Technische Universität Braunschweig/Mathematics, Berlin, DE

Abdel Douiri, UCL/Computer Science, CMIC, London, UK

David Holder - UCL/Medical Physics, Neurophysiology, London, UK

Simon Arridge, UCL/Computer Science, CMIC, London, UK